Icarus 265 (2016) 125–138

Contents lists available at ScienceDirect

Icarus

journal homepage: www.journals.elsevier.com/icarus

Observations and modeling of northern mid-latitude recurring slope lineae (RSL) suggest recharge by a present-day martian briny aquifer

David E. Stillman [a,*], Timothy I. Michaels [b], Robert E. Grimm [a], Jennifer Hanley [a,c]

[a] Dept. of Space Studies, Southwest Research Institute, 1050 Walnut St. #300, Boulder, CO 80302, USA
[b] Carl Sagan Center, SETI Institute, 189 Bernardo Ave, Suite 100, Mountain View, CA 94043, USA
[c] Lowell Observatory, 1400 W. Mars Hill Rd., Flagstaff, AZ 86001, USA

ARTICLE INFO

Article history:
Received 4 June 2015
Revised 7 October 2015
Accepted 8 October 2015
Available online 23 October 2015

Keywords:
Mars, surface
Geological processes
Mars, climate

ABSTRACT

Recurring slope lineae (RSL) are narrow (0.5–5 m) dark features on Mars that incrementally lengthen down steep slopes, fade in colder seasons, and recur annually. These features have been identified from the northern to southern mid-latitudes. Here, we describe how observations of northern mid-latitude RSL in northern Chryse Planitia and southwestern Acidalia Planitia (CAP) suggest that brines start flowing before northern spring equinox and continue for more than half a Mars-year (490 ± 40 sols, spanning solar longitude 337° ± 11°–224° ± 20°). All CAP RSL are found on the steep slopes of craters and their source zones are at or below the elevation of the surrounding plains. Spacecraft-derived surface temperature observations cannot resolve individual RSL, so thermal modeling was used to determine that CAP RSL have a freezing temperature of 238–252 K, freeze and melt diurnally, and flow only occurs within the top ~8 cm of the regolith. Furthermore, we calculate that a typical CAP RSL has a water budget of 1.5–5.6 m^3/m of headwall. Therefore, such a large water budget makes annual recharge via atmospheric or subsurface diffusion sources unlikely. Alternatively, we hypothesize that the most plausible RSL source is a briny aquifer with a freezing temperature less than or equal to the mean annual CAP surface temperature (220–225 K). The annual cycle is as follows: in late autumn, the shallowest part of the brine feeding the source zone freezes, forming an ice dam. As spring approaches, temperatures rise and the dam is breached. Brine is discharged and the RSL initially lengthens rapidly (>1.86 m/sol), the lengthening rate then slows considerably, to ~0.25 m/sol. Eventually, the losses equal the discharge rate and the RSL reaches its equilibrium phase. As brine flows in the RSL some of the water is lost to the atmosphere, therefore the freezing temperature of the brine within the RSL is higher (238–252 K) as the brine transitions to a super-eutectic salt concentration. In the late autumn, falling temperatures restore the ice dam and the H_2O in the RSL slowly sublimates away. Overall, CAP RSL possess a significantly different seasonality and much longer duration than typical southern mid-latitude RSL, suggesting that RSL at different latitude bands have different source types. Lastly, CAP RSL are the best evidence that shallow groundwater may still exist on Mars.

1. Introduction

Recurring slope lineae (RSL) are defined as narrow features ~40% darker than their surroundings and have three general characteristics: they incrementally lengthen down steep slopes during warm seasons, fade during cold seasons, and recur every Mars year (McEwen et al., 2011, 2014a; Stillman et al., 2014). RSL sites continue to be identified in images from the High Resolution Imaging Science Experiment (HiRISE; McEwen et al., 2007) onboard the Mars Reconnaissance Orbiter (MRO). RSL sites have steep slopes, exposed rocks (likely outcropping bedrock), and low albedo (Fig. 1b). Evidence of surficial material transport has not been detected, although slumps have transported material in locations where RSL existed previously (McEwen et al., 2014b). At four southern latitude RSL sites, near-infrared hydration absorption band signatures have been detected and are consistent with hydrated salts (Ojha et al., 2015). About 200 candidate and confirmed RSL sites have been discovered, within the southern mid-latitudes (SML), Valles Marineris, equatorial highlands, and in northern Chryse Planitia and southwestern Acidalia Planitia (CAP) (Fig. 1a). Confirmed RSL have been observed to recur, fade, and incrementally lengthen, whereas candidate sites lack confirmation of all three of these characteristics, often due to a lack of repeat coverage. While RSL have been found at a large number of

* Corresponding author.
E-mail address: dstillman@boulder.swri.edu (D.E. Stillman).

http://dx.doi.org/10.1016/j.icarus.2015.10.007
0019-1035/© 2015 Elsevier Inc. All rights reserved.

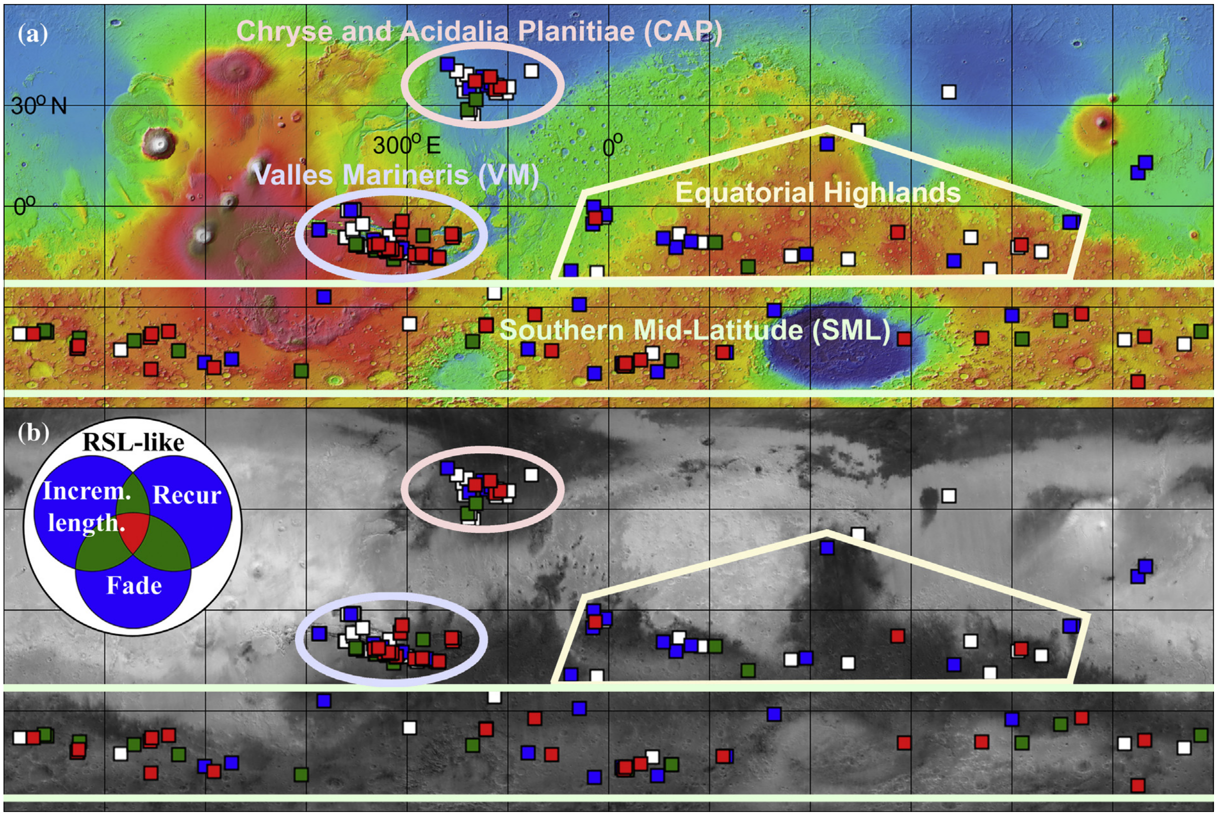

Fig. 1. Locations of candidate and confirmed RSL. Candidate and confirmed RSL are color-differentiated by the number of RSL-like characteristics (see inset Venn diagram) and plotted globally (latitude 60°S–60°N) on (a) Mars Global Surveyor (MGS) Mars Orbiter Laser Altimeter (MOLA; Smith et al., 1999) color-coded elevation and (b) Mars Global Surveyor (MGS) Thermal Emission Spectrometer albedo (Christensen et al., 2001). The four primary RSL regions are labeled.

sites, there are many other sites that seem to share the same external features but lack RSL (Ojha et al., 2014). Dry and wet origins have been suggested (McEwen et al., 2011), but water-based hypotheses best match observations that correlate incremental lengthening with higher surface temperatures (McEwen et al., 2011, 2014; Chevrier and Rivera-Valentin, 2012; Levy, 2012; Stillman et al., 2014; Grimm et al., 2014; Wang et al., 2015). However, surficial liquid water is only stable under optimal conditions when the pressure is above the triple point and the temperature is above the freezing point (Haberle et al., 2001; Hecht, 2002). In the shallow subsurface, temperatures are typically too cold for pure liquid water to persist (Burt and Knauth, 2003; Clifford et al., 2010). Brines increase stability, but pose other challenges in determining how the salt concentration and freezing temperature changes as water is lost and how salt is recharged.

The motivations of this paper are to constrain the formation and recharge mechanism of the CAP RSL and compare and contrast CAP RSL to SML RSL. We first describe the methodology of our data analysis (Section 2) and then detail our new observations (Section 3). We then test the interpretations of these observations with a thermophysical model to determine the likely salt concentration and water budget (Section 4). Next, we discuss the possible salt budget and type, each possible recharge and flow mechanism, and compare the CAP and SML RSL (Section 5). We conclude that the best match for CAP RSL formation and recharge is a briny aquifer (Section 6).

2. Methods

We used the Java Mission-planning and Analysis for Remote Sensing (JMARS; Christensen et al., 2009) to locate small (1–20 km) craters that were imaged by HiRISE in the northern mid-latitudes. We then analyzed high resolution (~0.3 m/pixel) HiRISE images to determine if RSL were visible and to establish the orientation of RSL-laden slopes. If other images of the same site are available within 90° of solar longitude (L_s), we then referenced the earlier images and categorized the change into one of four RSL categories: dark and lengthening, dark and static, partially faded, or completely faded (Stillman et al., 2014; all categorizations are given in Supplementary Information Excel-format file). If no images were available within 90° of L_s the image was categorized as either "dark but no recent images", or "completely faded". Note that "faded" is defined as when part of an individual RSL can no longer be distinguished from the lighter regolith around it. RSL sites were then characterized into candidate and confirmed locations. We examined each HiRISE image within our target region acquired between December 26, 2006 and July 12, 2015 or Mars year (MY; see Piqueux et al., 2015 for additional details) 28 L_s 155.9°–MY 33 L_s 12.0°.

To constrain the thermal conditions of RSL activity, surface temperatures of RSL locations were extracted from daytime data acquired by the Thermal Emission Spectrometer (TES; Christensen et al., 2001) onboard Mars Global Surveyor (MGS), from nadir measurements taken by MRO Mars Climate Sounder (MCS; McCleese et al., 2007; Hayne et al., 2012), and from 2001 Mars Odyssey Thermal Emission Imaging System (THEMIS; Christensen et al., 2004) brightness temperature retrievals. TES and MCS data have resolutions of ~3 km/pixel and THEMIS data have a resolution of 100 m/pixel, but none of these instruments are able to resolve individual RSL. Furthermore, their large pixel size can also result in biased surface temperatures due to heterogeneity (anisothermality) from sub-pixel variation in slope, rock abundance, and surface roughness (Christensen, 1986). TES and

MCS measurements were acquired in the afternoon at 13:00–14:42 and 13:54–15:36 local true solar time (LTST), respectively and produce the most robust temperature measurements. The TES data do not overlap temporally with HiRISE observations and were acquired from February 1999–October 2006 or MY 24 L_s 95°–MY 28 L_s 120°. MCS data overlap temporally with HiRISE observations, were taken at the same LTST, and were acquired over RSL sites from September 25, 2006–October 31, 2014 or MY 28 L_s 111.6°–MY 32 L_s 224.8°.

THEMIS data were measured at later times-of-day (14:45–18:12 LTST) and have not been collected in CAP between $L_s \sim 160°$ and 270°. At the CAP RSL sites, nearly all the THEMIS reduced thermal brightness temperature records are saturated in the Planetary Data System because they are scaled to 8-bit data for storage. Therefore, we reprocessed the raw data records to find the non-saturated values using the THEMIS processing web interface (THMPROC) in which only a signal drift correction was made. The maximum, mean, and minimum temperatures for each RSL site were computed by using THEMIS pixels that correlate with the geomorphological unit on which RSL form. THEMIS data overlap temporally with HiRISE RSL observations and were acquired over RSL sites from February 20, 2002–July 15, 2014 or MY 25 L_s 330.0°–MY 32 L_s 162.0°.

To determine the surface and subsurface temperature of the RSL throughout the day we used Mars Regional Atmospheric Modeling System (MRAMS; Rafkin et al., 2001; Michaels and Rafkin, 2008) in the vertical dimension only. This configuration of MRAMS is similar to other thermophysical models (e.g., KRC; Kieffer, 2013). Simulations include boundary layer turbulence and full atmospheric radiative transfer assuming a TES-based seasonal atmospheric dust loading (Michaels and Rafkin, 2008). MRAMS computes the subsurface state at 550 individual computational layers, with the layer thickness gradually increasing from 1 mm at the surface to ~1 cm at the bottom (2 m). We then assign thermal properties to groups of neighboring layers or zones (see Section 4.1 for further details).

To improve the realism of the thermal model, we varied the surface albedo as a function of season and used zones with thermal conductivity that not only changed as a function of season, but also with temperature and phase. The seasonal change is needed because water discharges into the RSL during the warm seasons and is absent in the cold seasons. The temperature/phase dependence is needed because the thermal conductivities of frozen and liquid water are quite different. Subsurface density and specific heat also varied appropriately in conjunction with the thermal conductivity. Furthermore, a significant amount of energy is consumed or liberated to complete a phase transition, and we therefore assigned a latent heat of fusion for each zone. Different salt types/mixtures were approximated by allowing freezing temperature values below 273.15 K. Latent heat of vaporization is not included in the MRAMS model because sublimation/evaporation rates are relatively low (e.g., Sears and Chittenden, 2005; Bryson et al., 2008) and simulation of these processes in porous media is more complex.

3. Observations and interpretations

RSL in the northern mid-latitudes of Mars are likely only detected in CAP (27.1–42.2°N; 312.2–337.0°E; elevation of −4000 ± 200 m) because higher albedo dominates the rest of this latitude band (Fig. 1b). Overall, we found 24 candidate and confirmed RSL sites (Fig. 2), 10 of which show incremental lengthening, and 4 confirmed sites that display all three RSL characteristics. All CAP RSL occur on relatively fresh craters (diameters 1–13 km), with no occurrences on the central peaks of large

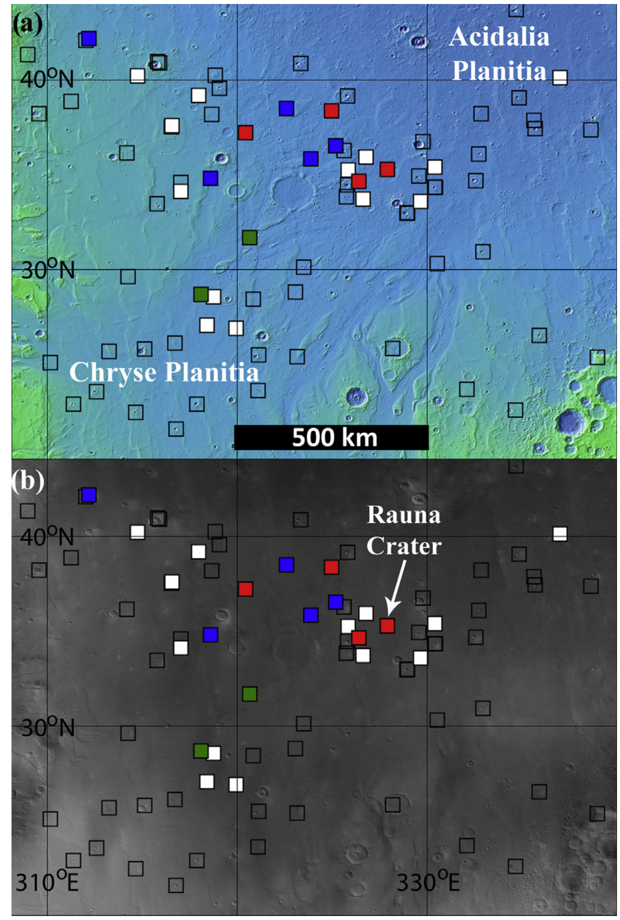

Fig. 2. Locations of candidate and confirmed RSL within CAP on (a) MGS MOLA color-coded elevation and (b) TES albedo. Candidate and confirmed RSL are color-differentiated by the number of RSL-like characteristics (see inset Venn diagram in Fig. 1). Boxes with no fill indicate sites for which HiRISE images are available, but that have no detectable RSL.

craters. CAP RSL are only found on southwest- and west-facing interior crater slopes. There is no obvious correlation between the slope facing direction and either latitude or crater diameter.

To date, Rauna crater is the only CAP RSL site with both orthorectified HiRISE images and a HiRISE-derived digital terrain map (DTM) with 1 m/pixel horizontal and a vertical precision of a few tenths of a meter (Kirk et al., 2008). We mapped all the major RSL at this site and found that the starting elevations of all the RSL are at or below the elevation of the surrounding plains (Fig. 3). Three other CAP sites have Mars Express High Resolution Stereo Camera (HRSC) DTMs with 75 m/pixel resolution and vertical precision of up to one pixel (Jaumann et al., 2007). At these sites, all RSL source at elevations at or below on the surrounding plains given the large vertical precision, Furthermore, CAP RSL source regions are never at the top of the crater wall.

Next, we determined the seasonality of when CAP RSL darken, lengthen, and fade, without regard to latitude, slope facing direction, or Mars year (Fig. 4). The data suggest that lengthening starts and stops at different times at different RSL sites. This is likely caused by stochastic differences in the thermal properties of each site and stochastic atmospheric phenomena (e.g., dust storms). The seasonality of the CAP RSL are summarized in Table 1 – as more data are acquired, the uncertainties of the current seasonal bounds should be reduced.

Our observations indicate that CAP RSL have a large initial lengthening rate, followed by a longer period of slower lengthening

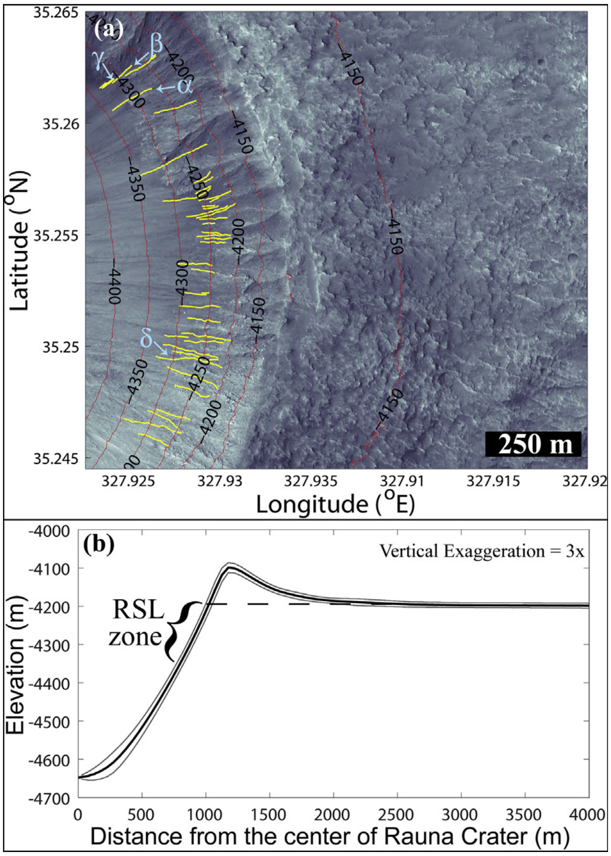

Fig. 3. (a) RSL in Rauna crater. (b) RSL start at a maximum elevation of −4200 m and end at a minimum elevation of −4350 m. The surrounding plains have an elevation of −4199 ± 7 m.

(Figs. 5 and 6). We quantified this behavior by measuring the largest distance an individual RSL traveled over the entire site (making this a maximum rate) between two HiRISE images and divided that by the number of sols between the images (Fig. 7a; maximum lengthening rates are given in Supplementary Information Excel-format file). Since Rauna crater has a HiRISE-derived DTM, we were able to convert the horizontal lengthening rates into true lengthening rates. For the other sites, we assumed a slope of 32.5° to convert from horizontal to true length. Overall, this analysis under-estimates the lengthening rate at the start and the end of the lengthening period, because it is likely that the RSL did not lengthen the sol immediately after the first image or up to the last image, respectively. The decrease in lengthening rate is clearly detected at the end of the lengthening period. However, the initial rate is much greater than the average lengthening rate, suggesting that the true starting lengthening rate may be >1.86 m/sol. For example, the maximum length of southwest-facing RSL in Rauna crater at MY 32 L_s 343.2° is 78.6 m. Unfortunately, we cannot determine when these RSL started to flow, but if we assume flow started early in the season at L_s 326° or 31 sols earlier than the maximum lengthening rate is ~4.33 m/sol. In the next image at MY 33 L_s 11° has a much slower lengthening rate of 0.21 m/sol. Overall, the large initial lengthening rate lasts for <100 sols at the beginning of spring (Fig. 7a). This rate then decreases considerably, with maximum rates of ~0.25 m/sol until late summer or ~270 sols (Fig. 4). RSL then remain static and dark for another ~120 sols until early fall when they fade.

We then compared the TES-, MCS-, and THEMIS-derived surface temperatures to CAP RSL seasonality and lengthening rate (Fig. 7b; Supplementary Fig. 1). Observed afternoon surface temperatures of CAP RSL sites are typically below the freezing point of pure water and have a mean TES temperature of 268 ± 11 K when lengthening (Table 1). Curiously, the highest lengthening rates correspond to the coldest measured TES surface temperature (240 ± 2 K) within the entire lengthening period. Furthermore, lengthening stops at a TES surface temperature of 276 ± 1 K and just after the yearly temperature peak at these locations. However, since CAP RSL are much smaller than the pixel size of the spacecraft-derived surface temperatures, sub-pixel heterogeneity effects limit the usefulness of these data.

By comparing the surface temperature and lengthening rate (Fig. 7), we hypothesize that the drastic decrease in the lengthening rate is caused by (1) a decrease in the rate at which brine is discharged from the source, and (2) seasonal variations in the amount of water vapor lost from an RSL. The evaporation and sublimation loss rates of an RSL vary directly with surface area and temperature. Therefore, the high initial lengthening rate values occur when

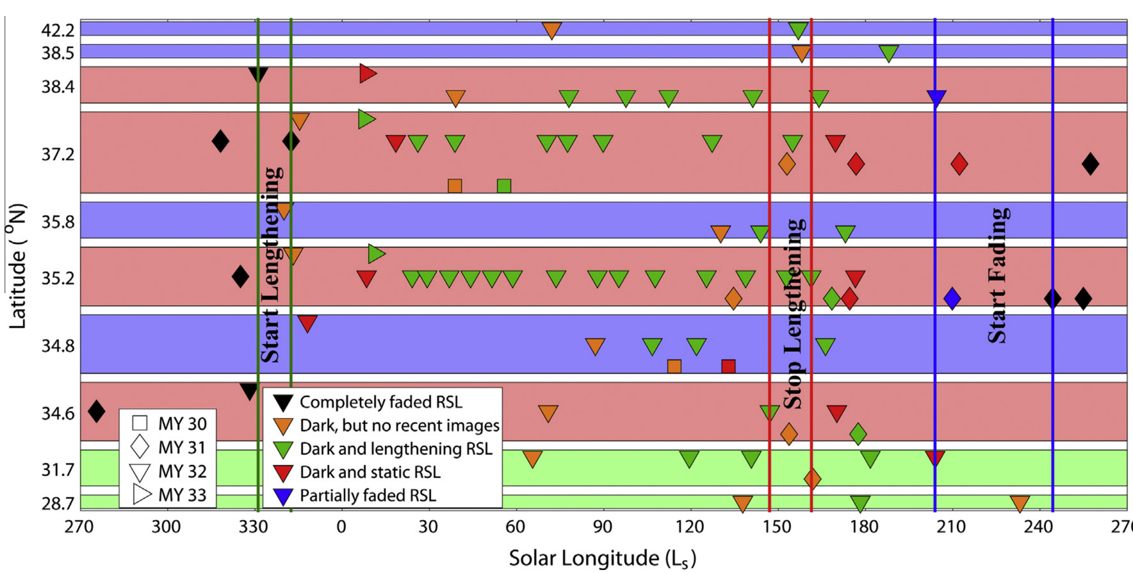

Fig. 4. Discrete CAP RSL HiRISE observations and their classification. RSL categories as a function of season are used to determine the duration. The lighter horizontal colored bands correspond to the Venn color scale in Fig. 1a. (For interpretation of the references to color in this figure legend, the reader is referred to the web version of this article.)

Table 1
Comparison of SML (Stillman et al., 2014) and CAP RSL. Temperatures are derived from TES afternoon observations, assuming RSL within their regions have repeatable behaviors every year.

	SML RSL			CAP RSL		
	L_s	Sols	Temperature (K)	L_s	Sols	Temperature (K)
Start lengthening	248° ± 11°		296 ± 2	337° ± 11°		240 ± 2
Stop lengthening	314° ± 12°		290 ± 3	154° ± 7°		276 ± 1
Start fading	16° ± 14°		245 ± 8	224° ± 20°		229 ± 9
Lengthening duration		104 ± 38	298 ± 3		369 ± 24	268 ± 11
Dark duration		220 ± 47	284 ± 16		487 ± 42	265 ± 13

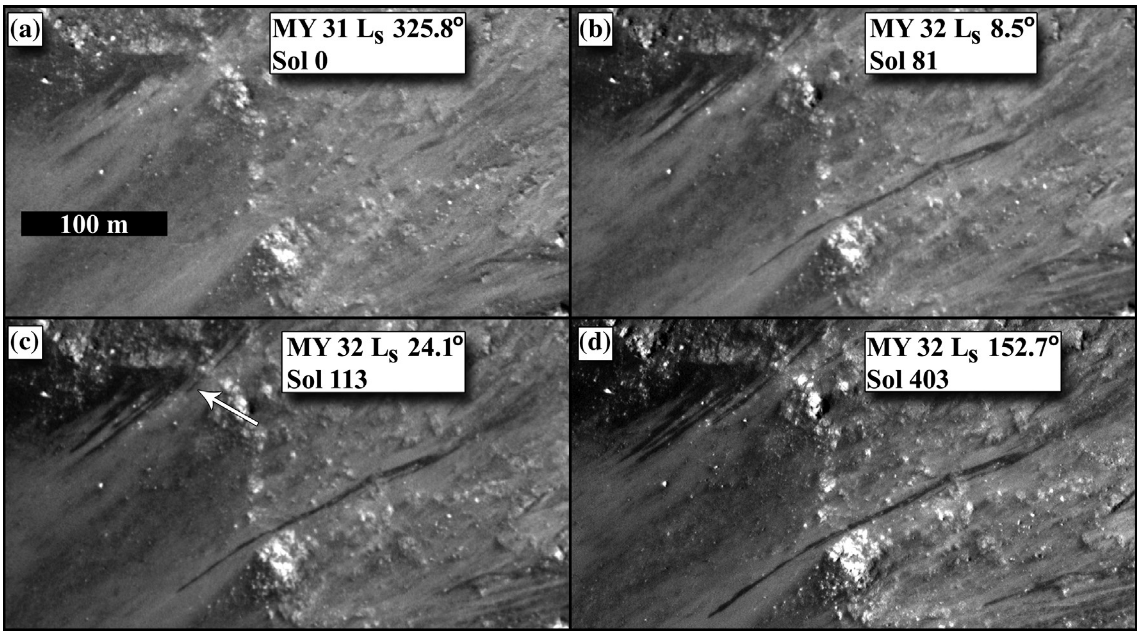

Fig. 5. Changing lengthening rates as a function of seasonality on a SW-facing slope at Rauna crater (35.26°N, 327.928°E). (a) No RSL are visible. (b) RSL have rapidly covered the surface. (c) RSL slowly lengthen. Arrow highlights most noticeable change. (d) RSL are at their longest length. Note that the image in (d) is not orthorectified, while the others are.

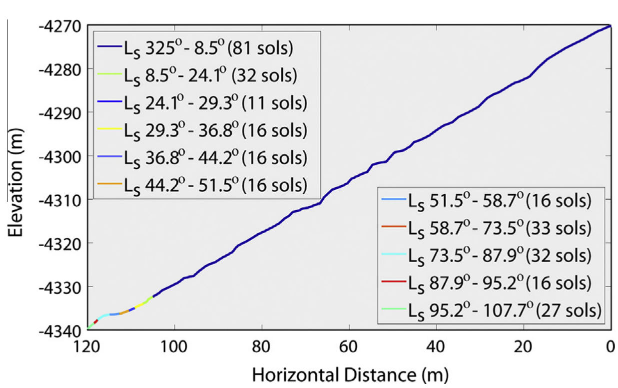

Fig. 6. Lengthening of RSL α as a function of season. 87% of the flow occurs between the first two images or 81 sols. The average slope of this RSL is 30.3°. Figure has a vertical exaggeration of 2.

these losses are minimal. As temperatures warm and the RSL becomes longer, the water vapor losses increase. This implies that an increasingly larger fraction of the water discharged into the RSL is only replenishing the water lost to the atmosphere, instead of allowing the RSL to advance. Eventually the sublimation and evaporation losses equal the discharge rate into the RSL and the RSL reaches an equilibrium flow state, as discussed by Grimm et al. (2014).

4. Modeling and analysis

4.1. Mars Regional Atmospheric Modeling System (MRAMS)

Observed surface temperatures are useful to correlate seasonal temperature variations with CAP RSL activity, but lack sufficient spatial and temporal resolution to differentiate between possible formation mechanisms. Therefore, we performed 1-D thermal modeling using MRAMS for southwest- and west-facing slopes at a slope angle of 32.5° to estimate the thermal/melt profile, given different configurations of subsurface thermophysical properties and melting temperatures. Each simulation is two Mars years in duration and is initialized with an isothermal subsurface temperature of 220 K. We modeled five CAP RSL sites as a function of latitude: 28.664°N, 318.102°E; 31.667°N, 320.658°E; 35.833°N, 323.892°E; 38.487°N, 324.983°E; 42.159°N, 312.210°E. The thermal properties of each layer were prescribed, using: (1) the lower Hashin–Shtrikman bound for the thermal conductivity of dry mixtures (Hashin and Shtrikman, 1962), (2) volumetric mixing for heat capacity, density, and saturated regolith thermal conductivity, and (3) modeled mixtures for the thermal conductivity of regolith containing salt-cementation and thin films (Piqueux and Christensen, 2009) (Table 2). The surface albedo is set at 0.09 when RSL are flowing and 0.15 when RSL are not visible (based on the maximum relative albedo difference between dark and completely faded RSL in McEwen et al., 2011). We varied the number of zones,

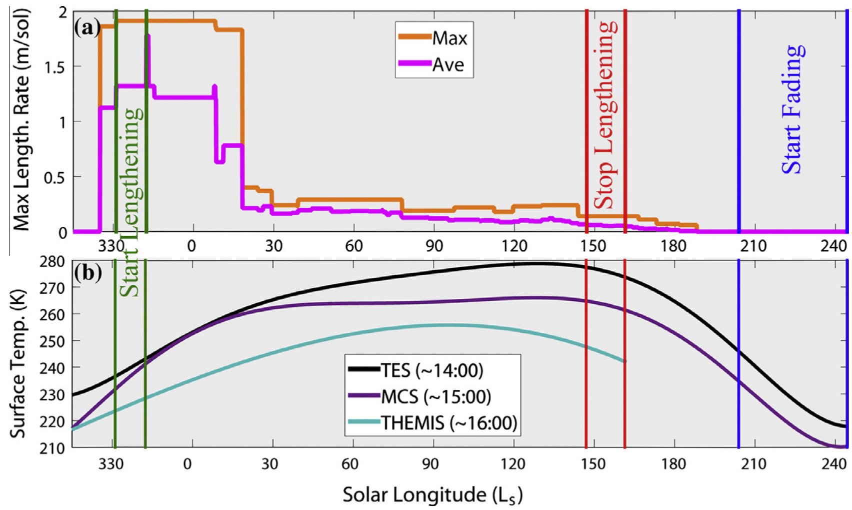

Fig. 7. CAP RSL seasonal cycle. (a) Maximum RSL lengthening rate as a function of season. These RSL have lengthen at an initially large rate, followed by a much longer period of slower lengthening. (b) Polynomial fits to spacecraft-derived surface temperature as a function of season (see Supplementary Fig. 1). Note that these measured afternoon temperatures do not actually represent the temperature of a CAP RSL, as none of these instruments have the necessary imaging resolution.

Table 2
Assumed thermal properties of units within modeled RSL. Ice- and brine-saturated regolith occur concurrently, with brines forming when/where the temperature is greater than the eutectic temperature. Note that the thermal properties assume a dry porosity of 45% for each layer. Between L_s 244° and 319° each zone's thermal properties were gradually transitioned from one state to the other.

Description	Zone number and solar longitude (L_s)	Conductivity (W m^{-1} K^{-1})	Heat capacity (J kg^{-1} K^{-1})	Density (kg m^{-3})	Thermal inertia (J m^{-2} K^{-1} $s^{-1/2}$)
Dry regolith	Zone 1: 319–331° Zone 4: 0–360°	0.084	837	1622	338
Water-films on regolith grains	Zone 1: 331–244°	0.64	1005	1738	1059
Salt-cemented regolith	Zone 2: 319–331°	0.777	837	1841	1094
Brine-saturated regolith	Zone 2 & 3: 331–244°	1.2	1093	2035	1634
Ice-saturated regolith	Zone 2: 331–244° Zone 3: 0–360°	2.49	1093	2035	2353

together with the thickness of the zones, and brine freezing temperature (the latent heat of fusion; Chevrier and Altheide, 2008) to find the model solution that best fit the observational constraints.

Numerous exploratory runs were conducted to determine a way to increase the temperature within the shallow subsurface while having a high but realistic thermal inertia of water- or ice-saturated regolith. We found that a homogeneous subsurface with the thermal properties of dry regolith can reach a maximum diurnal temperature above the freezing temperature of pure water. However, in a homogeneous subsurface of H_2O-rich saturated regolith with a freezing point of 238 K, brine will only melt from L_s 130° to 145°. This occurs because the thermal conductivity of the saturated regolith is an order of magnitude greater than that of its dry counterpart, which allows much more heat to be transported to greater depth instead of raising the surface temperature.

We then tested two-zone model runs. MRAMS cannot model evaporation or sublimation of water, but we infer that the top few centimeters cannot be saturated with liquid water as these layers experience the greatest evaporation and sublimation losses and highest temperatures. We therefore parameterize the top zone as having thermal properties consistent with dry regolith when RSL are not dark and regolith with films of water (~10 vol% or 12 monolayers on a surface with a specific surface area of 17 m^2/g) when dark (Table 2; Pommerol et al., 2013; Masse et al., 2014). These films are wicked from wetter layers below, have lower evaporation rates than free pore water, and likely change thickness throughout each sol (Möhlmann, 2010). These films also darken the surface (Pommerol et al., 2013) and increase grain-to-grain contact, thus increasing the amount of heat absorbed and conducted (Piqueux and Christensen, 2009). The second zone is parameterized as salt-cemented regolith when RSL are faded, and regolith saturated with brine or ice when RSL are dark. With a zone 1 thickness of 2 cm, the salt-rich ice never melts, even at a freezing point of 238 K. No melting occurred because zone 1 insulated zone 2 from large temperature variations. Furthermore, much of the heat that entered zone 2 was quickly conducted away, preventing thawing.

To keep more solar energy nearer to the surface we then added a dry zone to the bottom of the model that was parameterized as a thermally-insulating dry unconsolidated regolith in order. We assumed that since RSL form on fan deposits and drainages, deeper parts would never have consolidated and the brine from the RSL could never have penetrated to or persisted at these depths. These model runs produced reasonable results for freezing temperatures (T_f) of 238 and 252 K. While three-zone models were thermally reasonable, they were not hydrologically likely because as the RSL advanced downslope there was no competent layer to act as an aquitard and stop/retard the brine from flowing into the deeper subsurface (minimizing any surface expression).

Four-zone model configurations were then run, by breaking the second zone (saturated with water/ice) into two zones. Therefore, the second (of four) zones possesses thermal properties of regolith that is water/ice saturated when RSL are dark and salt-cemented regolith when RSL are faded. The third zone is parameterized as regolith that is water/ice saturated for the entire year and is above the fourth perennially-dry zone. While the third layer is allowed to melt, we only accept models where this implied impermeable boundary or aquitard never fully melts. This deep impermeable frozen layer is assumed to remain throughout the year, and is only stable because sublimation rates are small because it is cold, deep, and only has to persist for ∼180 ± 50 sols ($L_s \sim 224 \pm 20°$–$337 \pm 11°$) before it is replenished by the following year's flow. The thicknesses of the four zones were adjusted so that melt occurred over the observed seasonal range (Table 3; Figs. 8–11). Model runs with brine T_f of 238–252 K produced acceptable results. This constrains the dominant salt type to be a chloride, chlorate, or perchlorate as these are the Mars-relevant salts that have eutectic temperature less than the modeled T_f range (Fig. 12). Therefore, sub-eutectic concentrations of salt must reach >10 wt% to obtain such a large T_f. Furthermore, even higher salt concentrations (up to 60 wt%) are needed to reach super-eutectic temperatures where salt hydrates precipitate out (Fig. 12). While a non-eutectic concentration would still have some liquid below

Table 3
Vertical cross-sections of modeled RSL. These configurations best fit the duration limits of melt (Table 1) at latitude 35.833°N and longitude 323.892°E (a confirmed RSL site near the middle of the CAP RSL region). Southwest-facing slopes are warmest, therefore they have thicker top (insulating) zones. Zone 3 was used to adjust the duration length, but was always thick enough to ensure its role as an aquitard. Note that zones 1 and 2 grade from volatile-rich to volatile-poor between L_s 244° and 319° and rapidly become volatile-rich at L_s 331°.

Eutectic temp. (K)	Latent heat of fusion (kJ/kg)	Orientation	Zone depth (cm)	Zone description
252	31.0	SW-facing	0–2.5 2.5–4.4 4.4–5.7 5.7–∞	Thin films on regolith grains → Dry regolith Ice/brine-saturated regolith → Salt-cemented regolith Ice/brine-saturated regolith Dry regolith
252	31.0	W-facing	0–1.9 1.9–3.0 3.0–4.1 4.1–∞	Thin films on regolith grains → Dry regolith Ice/brine-saturated regolith → Salt-cemented regolith Ice/brine-saturated regolith Dry regolith
238	29.19	SW-facing	0–2.0 2.0–3.9 3.9–22.8 22.8–∞	Thin films on regolith grains → Dry Ice/brine-saturated regolith → Salt-cemented regolith Ice/brine-saturated regolith Dry regolith
238	29.19	W-facing	0–1.2 1.2–2.5 2.5–7.0 7.0–∞	Thin films on regolith grains → Dry regolith Ice/brine-saturated regolith → Salt-cemented regolith Ice/brine-saturated regolith Dry regolith

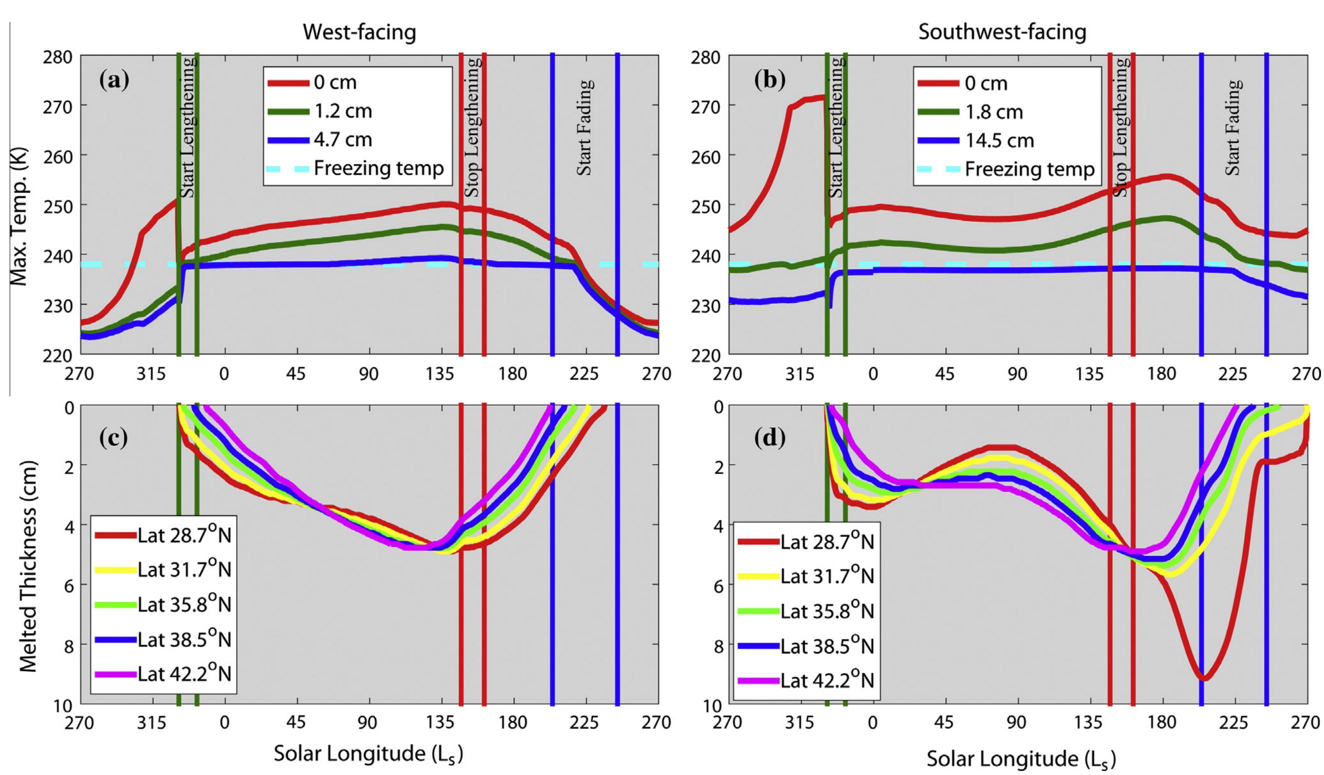

Fig. 8. Modeled maximum temperature and melted thickness for a T_f = 238 K. Maximum diurnal temperature as a function of season and depth for (a) west-facing and (b) southwest-facing slopes at 35.833°N, 323.892°E. Depths represent the surface, top of zone 2, and middle of zone 3. Maximum melted thickness as a function of latitude for (c) west-facing and (d) southwest-facing slopes. West-facing slopes slowly increase in temperature until reaching a maximum (∼L_s 135°). Southwest-facing slopes are more sensitive to latitude and warm quickly, then relax to a temperature minimum (∼L_s 80°), and then reach a second maximum near L_s 180°.

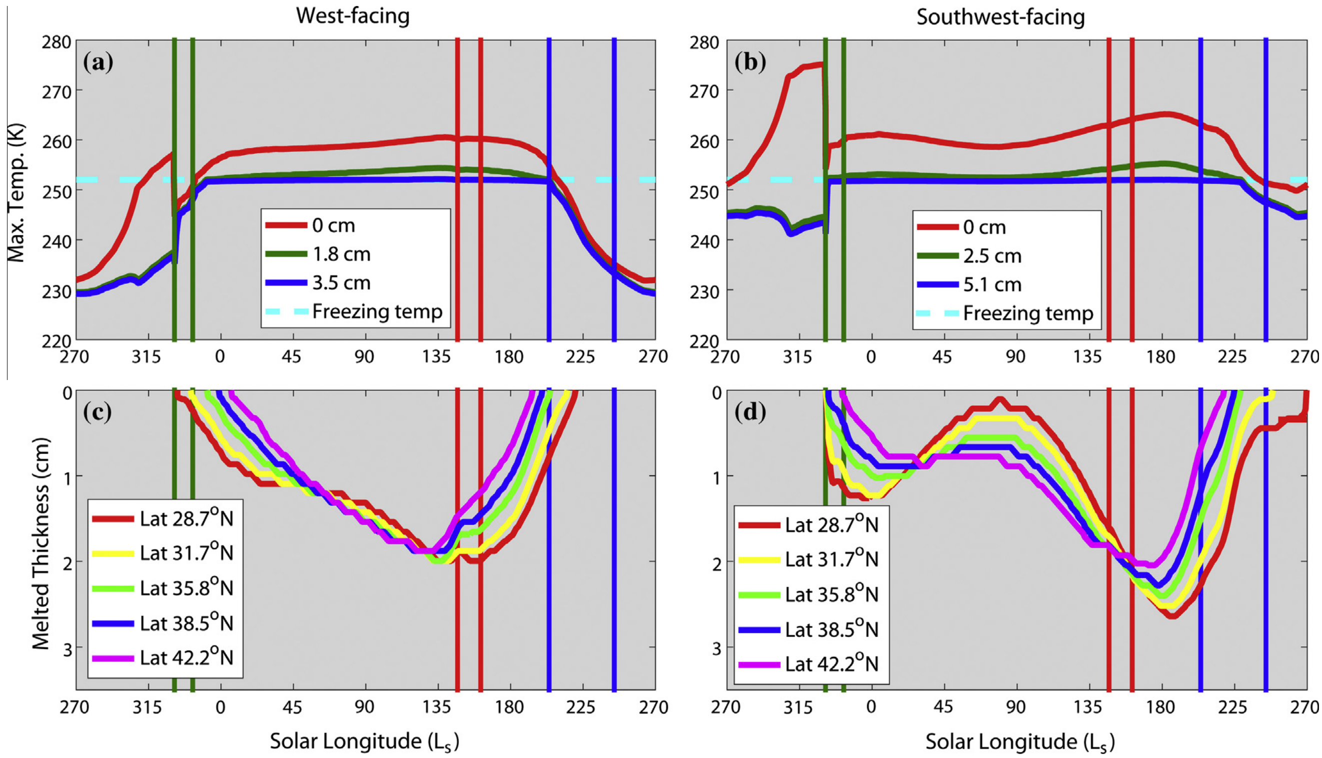

Fig. 9. Modeled maximum temperature and melted thickness for a $T_f = 252$ K. Maximum diurnal temperature as a function of season and depth for (a) west-facing and (b) southwest-facing slopes at 35.833°N, 323.892°E. Depths represent the surface, top of zone 2, and middle of zone 3. Maximum melted thickness as a function of latitude for (c) west-facing and (d) southwest-facing slopes. West-facing slopes slowly increase in temperature until reaching a maximum (~L_s 135°). Southwest-facing slopes are more sensitive to latitude and warm quickly, then relax to a temperature minimum (~L_s 80°), and then reach a second maximum near L_s 180°.

its T_f but above its eutectic temperature, the permeability would decrease due to pore-filling ice or salt hydrates. Our models also suggest that brine freezes and remelts every sol (Figs. 10 and 11). Model simulations with $T_f = 252$ K produced only ~2 cm of maximum melt and thus are considered to be an upper limit on plausible T_f. SW-facing model runs with $T_f = 238$ K required a volatile-rich layer thick enough so that they would not melt through the aquitard (zone 3), but not so thick that melt persisted to the winter solstice. Brine with T_f less than or equal to the mean CAP annual surface temperature of 220–225 K produces melt year-round, and thus these low T_f models were discarded.

Our modeling also showed that the maximum surface temperature while RSL are darkening is not reached until ~14:15 LTST for southwest-facing slopes ($T_f = 238$ K), ~15:30 LTST for west-facing slopes ($T_f = 238$ K), ~15:00 LTST for southwest-facing slopes ($T_f = 252$ K), and ~15:30 LTST for west-facing slopes ($T_f = 252$ K). Note that west-facing slopes do not reach their maximum temperature until later the day because they receive less morning insolation than southwest-facing slopes. This suggests that HiRISE observations, which are typically acquired at ~14:45 LTST, may be imaging RSL near their maximum diurnal temperature.

4.2. Water budget calculation

To calculate the volume of water released from a typical CAP RSL, we parameterized the evaporation and sublimation rate on Mars, E (unit: (cm of H_2O) s^{-1}), as a function of temperature T (Ingersoll, 1970; Sears and Chittenden, 2005) and burial depth D (Bryson et al., 2008 assuming an overburden with a sand grain size of 125–250 μm):

$$E = (3.0 \pm 0.5) \times 10^{-21} \exp(0.115T)/D \qquad (1)$$

Note that the error in this empirical equation primarily comes from the uncertainties in the sublimation versus depth measurements (Bryson et al., 2008), and this equation is only valid over a depth range of 1–5 cm. For T, we used the temperature output of the MRAMS model at the top of the saturated zone when CAP RSL were flowing (L_s 331–244°). The depth to the top of the saturated zone was used for D. We calculated E and multiplied it by the incremental time (typically ~20 Mars-min) between the temperature values to estimate the total evaporation/sublimation loss when RSL are flowing. Note that we do not discriminate between evaporation or sublimation losses as the difference between the two is small compared to other uncertainties in the water budget. This analysis assumes that the RSL are always at maximum surface area, which is a reasonable approximation as RSL initially rapidly surge to long lengths before decreasing their rate of advance. Furthermore, the evaporation/sublimation loss calculation also does not include any losses from thin films that are constantly wicking water. However, we assume these losses should be minor as films are volumetrically small and their evaporation rate should be considerably smaller than free water since they are hydrogen bonded to the surface of the pores. To find the total evaporation/sublimation loss during the off-season, we multiplied the thickness of zone 2 (volatile-poor when RSL are faded) by its porosity (0.45). The off- and active-season losses were then added together, with the active-season losses equaling ~90% of the total evaporation/sublimation loss. We modeled 20 different scenarios (5 different latitudes, 2 different freezing temperatures, and 2 slope facing orientations) and found that the total annual water loss from a 1-D column was 6.2 ± 1.9 and 9.1 ± 2.5 cm when T_f was 238 and 252 K, respectively. The same zone thicknesses were used at each latitude, but differed for different freezing temperatures and slope facing orientation (Table 3). The thickness of zones 1 and 2

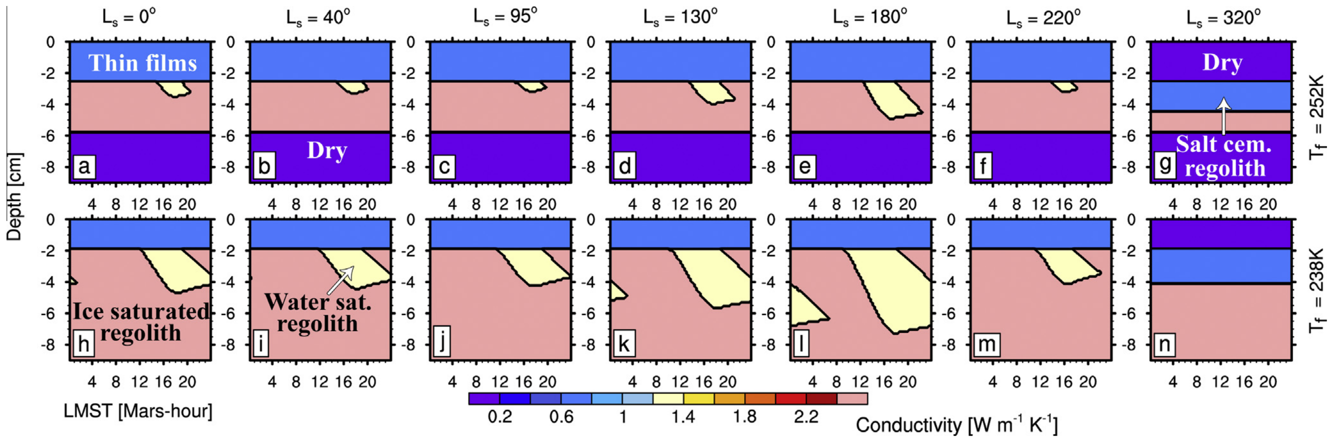

Fig. 10. RSL cross-section showing melt as a function of depth and time-of-day for southwest-facing slopes. Modeled assuming a eutectic temperature of 252 K (a–g) and 238 K (h–n). The melt thickness reaches a minimum around L_s 95° and reaches its maximum value at L_s 180°. Note that the ice-saturated zone extends down to 25 cm in the 238 K model.

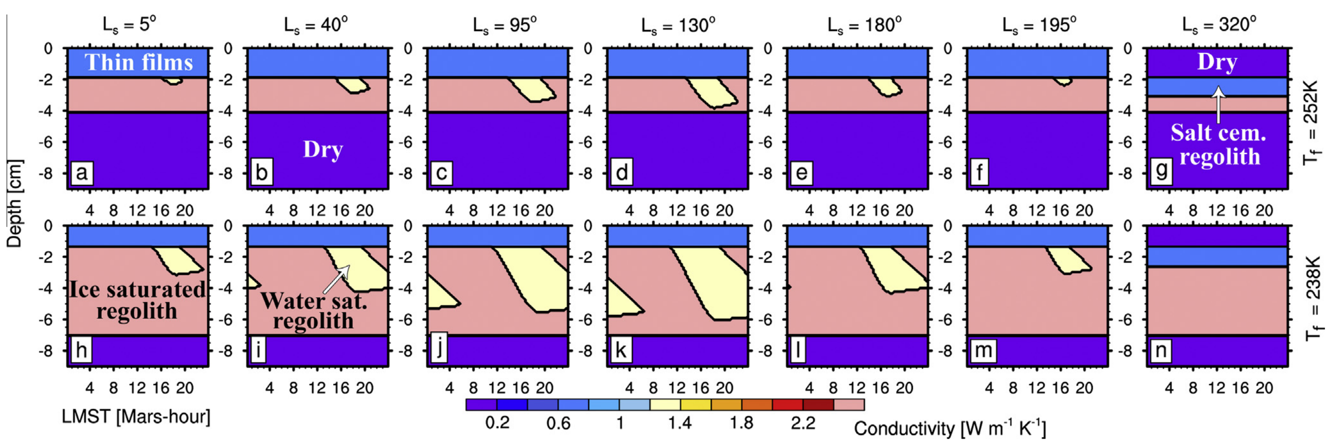

Fig. 11. RSL cross-section showing melt as a function of depth and time-of-day for west-facing slopes. Modeled assuming a eutectic temperature of 252 K (a–g) and 238 K (h–n). The melt thickness slowly increases until it reaches its maximum value around L_s 130°.

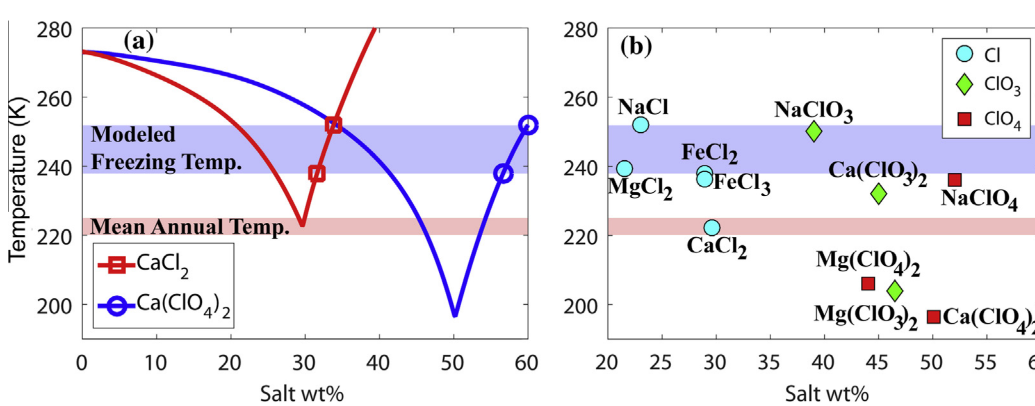

Fig. 12. (a) Temperature as a function of salinity for two candidate salts: $CaCl_2$ and $Ca(ClO_4)_2$. The phase diagram at sub-eutectic concentrations represents the freezing temperature, while a super-eutectic concentrations the curve represents the temperature at which salt hydrates precipitate. Our hypothesis assumes that as the ancient aquifer freezes, salt is excluded and the salinity increases until the mean annual temperature is reached. The brine then discharges into the shallow-subsurface (<10 cm) and increases its salinity as H_2O is lost to the atmosphere. Therefore, CAP RSL brine concentrations are hypothesized to be super-eutectic. For example, a $CaCl_2$ aquifer would have a salt concentration of 30 wt% and then within the RSL water loss would increase the salt concentration to ~32.5 wt%. (b) Eutectic temperature and composition of other candidate salts ($FeCl_2$ – Marion et al., 2003; $FeCl_3$ – Marion et al., 2008; all ClO_3 – Hanley et al., 2012; $NaClO_4$ and $Mg(ClO_4)_2$ – Chevrier et al., 2009; $Ca(ClO_4)_2$ – Nuding et al., 2014). Note that only salts with a eutectic temperature less than the mean annual temperature would be practical under the briny aquifer hypothesis.

decreases with decreasing T_f and the thickness of zone 3 (volatile-saturated aquitard directly under the RSL) was varied to best match RSL duration and to ensure the presence of an always-frozen bottom aquitard. Thus, the thickness of zone 3 increases with decreasing T_f. Overall, west-facing slopes lost ~20% more water than southwest-facing slopes, west-facing slopes lost ~10%

more water at 28.664°N compared to 42.159°N, and southwest-facing slopes lost ~5% more water at 42.159°N compared to 28.664°N. It appears that southwest-facing slopes lost more water at higher latitude because the brine was able to stay liquid longer because the length of daylight was longer at higher latitudes.

Next, we calculated the surface area of the RSL once it had reached its longest length, then divided by its source headwall. This was done for 13 CAP RSL, finding an average ratio of 44 ± 5 m^2/m. This average ratio was multiplied by the total annual water loss to yield the normalized water budget of 2.7 ± 1.2 and 4.0 ± 1.6 m^3/m for T_f = 238 and 252 K, respectively. Grimm et al. (2014) first recognized that total throughput could far exceed visible RSL. Therefore, we calculate the water loss-to-storage (where storage is the amount in the pore space) ratio by taking the yearly water loss and dividing it by the thickness of zone 2 multiplied by the porosity. This yields a loss-to-storage ratio of 3.9 ± 2.1 and 6.1 ± 3.1 for T_f = 238 and 252 K, respectively.

5. Discussion

5.1. Salt budget and type

CAP RSL start flowing when temperatures are too cold for pure water flows, so these flows must emanate as brine from their source. Therefore, any volatile recharge mechanism for CAP RSL must address how salt is recharged. The annual recurrence of RSL flows indicates that any salt originally resident in the source zone should have been flushed out. Furthermore, there is no evidence for present-day mass wasting at RSL source zones, which would potentially make new salt deposits available on a regular basis. Our MRAMS model runs that best fit the observed durations require a T_f range of 238–252 K. Therefore, the only constraint on salt type we can provide is that it must have a eutectic temperature ⩽252 K. This indicates chloride (Cl^-), chlorate (ClO_3^-), and/or perchlorate (ClO_4^-) salts and excludes the most likely types of sulfate and carbonate salts, as they have higher eutectic temperatures. The salt concentration within a CAP RSL would be 20–60 wt% assuming Cl^-, ClO_3^-, and/or ClO_4^- salts (Fig. 12b). Once flow ceases because the available energy can no longer fully melt the brine, the resultant salt-hydrate–brine–ice mixture loses its H_2O through sublimation. The remaining salt would then remain in the pore space along the RSL track. Future brine flows would have difficulty dissolving this salt, and eventually such remnant salt would act as an impermeable boundary for future RSL flows.

Note that the salt involved in the CAP RSL is likely not a single species, but rather a mixture of many cations (Na^+, Mg^{2+}, Ca^{2+}, and/or $Fe^{2+/3+}$) and anions (Cl, ClO_3, and/or ClO_4). Such a mixture of salts would decrease the eutectic temperature below that of the individual eutectic temperatures (e.g., Hanley et al., 2012). For T_f = 238 and 252 K, brine densities vary from 1190–1260 and 1160–1190 kg m^{-3} (CRC, 2008), respectively for Cl^-, ClO_3^-, and ClO_4^- salts. This produces a significant salt budget of 1800–4900 or 2800–6700 kg per m of headwall for T_f = 238 or 252 K, respectively. Assuming a density range of 2150–2700 kg m^{-3} for non-Fe anhydrous salts (CRC, 2008), we find a salt volume of 0.7–3.1 m^3/m. This is a remarkable amount of salt, therefore any explanation must explain how water is recharged and how salt is lost and recharged.

5.2. Recharge mechanisms

5.2.1. Atmospheric water vapor

The atmosphere is a plausible source as it transports water all over the planet (McEwen et al., 2015). However, RSL activity does not correspond with increased atmospheric water vapor (McEwen et al., 2014a, 2014b) and no mechanism has been found to effectively trap enough atmospheric water in the subsurface. The martian atmosphere just cannot hold much water vapor (typically ~5–10 precipitable-μm/m^2; Davies, 1979) due to its low average temperature and so a given RSL site would have to be both effective at dewatering the atmosphere and have a great amount of air pass over it (Grimm et al., 2014). At 50% trapping efficiency, ~0.7 km^2 of martian atmosphere is required to satisfy the CAP RSL water budget. This efficiency is likely an overestimate because some, if not most, of the condensed water will sublimate before it can be melted. Therefore, the actual requirement of atmospheric water involved must be considerably greater than this estimate.

An intriguing terrestrial analog to RSL are the Antarctic water tracks, where hygroscopic salts deliquesce and partially source these seasonal flow features (Levy, 2012; Dickson et al., 2013). However, the majority of these flows are sourced from snow, unlike Mars. Furthermore, many of these dark features actually fade during the daytime when the humidity decreases (Dickson et al., 2013). While others have shown deliquescence is possible during the pre-dawn and early morning hours on Mars (Gough et al., 2011; Nuding et al., 2014; Wang et al., 2015; Martin-Torres et al., 2015), no research has shown that deliquescence can exist at the surface when temperatures are near their daily maximum, relative humidity is at its lowest point, and the HiRISE RSL observations are made. Furthermore, the idea of RSL deliquescence raises many more difficult questions that current observations do not support: (1) Why would the albedo features fade when relative humidity rises in the winter? (2) If previous flows had already deposited salt downslope, why wouldn't the entire RSL darken once some humidity threshold was reached? (3) After many years of lengthening how would salt at the headwall be recharged? (4) How did RSL areas become so enriched in this hygroscopic salt compared to other areas? Overall, deliquescence is likely occurring within RSL, but it does not appear to be able to sequester the necessary volume of water needed to seasonally initiate RSL.

5.2.2. Vapor migration from subsurface ice

CAP and SML RSL are in regions with latitude-dependent mantling (LDM; Kreslavsky and Head, 1999; Mustard et al., 2001) and concentric crater fill (CCF; Levy et al., 2010) suggesting that subsurface ice is in close proximity. Without annual mass wasting the RSL sources cannot just be the melting of this ice, as any ground ice within the annual melting zone would be quickly depleted. Therefore, Stillman et al. (2014) and Grimm et al. (2014) investigated how annual subsurface transport of water vapor from a deeper volatile source to a nearer-surface frozen reservoir could potentially be the source of SML RSL. They found that not enough water vapor could be transported, because of cold temperatures and the flow of water vapor is restricted mostly by CO_2 gas in the subsurface. Even an assumption that the subsurface is warm (~273 K) and CO_2-free still does not allow enough water to be trapped in the SML RSL source regions, which have ~565 sols to recharge. As the CAP RSL have even less time (~180 sols) to recharge, this mechanism seems unlikely. Also, only water can be transported as vapor, and thus a separate salt recharge mechanism would be needed for the briny CAP RSL.

5.2.3. Aquifer

The last recharge mechanism we consider is a briny aquifer. There is abundant evidence of ancient aquifers on Mars (e.g., Grotzinger et al., 2005; Andrews-Hanna and Lewis, 2011; Michalski et al., 2013), but it is unknown if any aquifers persist currently (Grimm and Painter, 2009; Clifford et al., 2010). The Mars Express Mars Advanced Radar for Subsurface and Ionosphere Sounding (MARSIS) and the MRO SHAllow RADar (SHARAD) were designed to detect aquifers. However, most rocky surfaces have proved to be opaque to both MARSIS and SHARAD. This indicates either that there are no large interfaces to create reflections or the subsurface is more attenuative than was originally assumed (Stillman and Grimm, 2011). We assume the latter because it is likely that near-surface groundwater in the late Noachian–early Hesperian produced clays and other alteration products that increase radar attenuation (Stillman and Grimm, 2011) compared to dry minerals (e.g., Stillman and Olhoeft, 2008). Therefore a null result from orbital radar does not rule out the existence of aquifers (Farrell et al., 2009). Furthermore, the orbital gamma ray or neutron spectroscopy would not detect the presence of a subsurface aquifer if it was buried by more than a few tens of cm of regolith. Moreover, RSL themselves are much too small for detection with orbital gamma ray or neutron spectroscopy as a pixel is ~600 km (Prettyman et al., 2004).

Previous hypotheses for gully formation via groundwater used low thermal conductivities and/or high heat flow to allow “warm” aquifers to exist at depths of ~100 m (Mellon and Phillips, 2001; Goldspiel and Squyres, 2011). This is plausible for gully formation as the water is rapidly released (100s m^3 per sol; Goldspiel and Squyres, 2011) from the aquifer via a fracture. This formation mechanism does not work for an RSL because water flowing through a crack in the cryosphere discharges slowly and would freeze. Furthermore, there is no mechanism that would keep the deeper portion of such a liquid-filled crack from freezing during the inactive season and there is no mechanism to remelt it or form a new crack each year. The only way to keep the water in the fracture is to allow it to have an aquifer freezing temperature at or below the mean annual temperature – if this is the case there is no need to invoke low thermal conductivity materials or high heat flow.

Another way to make a shallow aquifer is to melt subsurface ice via impact-induced heating (e.g., Schwenzer et al., 2012). This appears to produce hydrothermal systems in craters that impact a volatile-rich material and are >5 km in diameter on Mars (e.g., Newsom et al., 2001; Schwenzer et al., 2012), while the CAP RSL occur within small impact craters (diameter 1–13 km). However, the duration of hydrothermal activity after crater formation for crater diameters from 5 to 13 km is 300–100,000 yr (see compilation in Rummel et al., 2014). Therefore, this mechanism could work for the larger craters, but it cannot explain why RSL occur in craters less than 5 km in diameter and why there would be so many recent craters in CAP.

Global groundwater models suggest that groundwater under CAP would have been close to the surface and may have been actually discharging water onto the surface in the late Noachian–early Hesperian CAP (Andrews-Hanna and Lewis, 2011). Furthermore, the mineralogy suggests at Meridiani Planum (Grotzinger et al., 2005; Andrews-Hanna et al., 2007, 2010) and in McLaughlin crater (337.6°E, 21.9°N; Michalski et al., 2013) was likely altered by the existence of large groundwater systems. The original salt content of this ancient aquifer determines if this aquifer is currently unconfined or confined.

If the late Noachian–early Hesperian CAP aquifer originally had a high salt content with freezing temperature lower than the current mean annual temperature, then as water was lost via evaporation, an impermeable duricrust layer between the surface and the aquifer would have been produced. Thus lowering the evaporative losses. The HiRISE-derived DTM at Rauna crater suggests that this near-surface unconfined briny aquifer could simply discharge via springs to form the CAP RSL (Fig. 13a). RSL do not flow year round because in the winter the near-surface temperatures drop below the freezing temperature of the aquifer creating an ice dam. As northern spring approaches solar insolation/warming increases, eventually breaching the ice dam.

If the ancient CAP aquifer originally had a low salt content with freezing temperature higher than the current mean annual temperature, then as the surface and subsurface cooled, the top of the aquifer would have begun to freeze (Fig. 13b). This produces an impermeable cap of near-surface ice that excludes salt back into the aquifer. Therefore, the salinity of the aquifer increases as more ice is formed (e.g., Burt and Knauth, 2003). However, the increase in salinity is likely primarily controlled by the water alteration (e.g., leaching) of host rock. Furthermore, cation exchange is expected to occur and would favor an enrichment of Ca^{2+} over Na^+ (e.g., Knauth and Burt, 2002). All these factors lead to a lower freezing temperature and it is possible that the brine may even reach its eutectic concentration (Fig. 12; Burt and Knauth, 2003). Furthermore, the freezing of ice could have pressurized and confined the remaining brine (e.g., Carr, 1979; Wang et al., 2006). As freezing continued, this pressurization could have raised the aquifer's current potentiometric surface to the CAP RSL elevations (Fig. 13b).

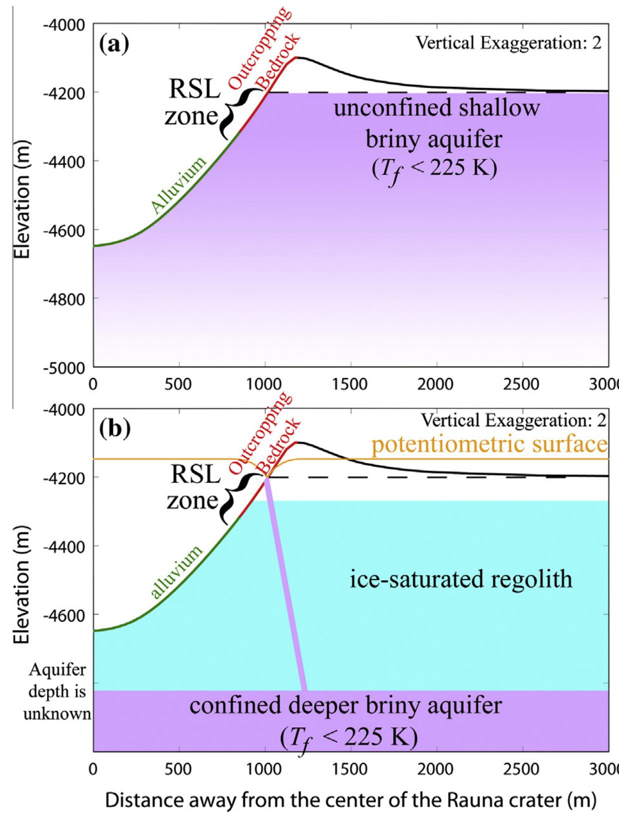

Fig. 13. Schematics of our favored aquifer recharge mechanisms. RSL are sourced at or below the surrounding plain elevation. RSL emanate from or in proximity to bedrock outcrops and flow into the alluvium below. In the Noachian to Early Hesperian an unconfined aquifer lay near the surface of CAP. (a) If this ancient aquifer were briny (T_f < 225 K), then as water evaporated away a duricrust would have formed in the soil above the aquifer, thus allowing it to survive within a few meters of the surface today. Furthermore, this aquifer could also be stable thermally if it had a freezing point less than or equal to the mean annual surface temperature. Note that the thickness of this unconfined briny aquifer is unknown. (b) If this ancient aquifer were not briny, then as the surface cooled, the top of the aquifer would have begun to freeze. The expansion of ice pressurized the aquifer. Salt would then be excluded from the ice, thus concentrating into the aquifer. However, a greater quantity of salts may have been obtained from bedrock leaching. After crater formation, fractures penetrating the pressurized briny aquifer would allow brine to discharge, thus forming CAP RSL. Note that as brine is discharged, the potentiometric surface drops to the elevation of the fracture discharge point.

Travis et al. (2013) modeled the implications of freezing a salty ($CaCl_2$) aquifer and showed that hydrothermal circulation can deposit brine close to or at the surface. We infer that the brine reaches the surface via a bedrock fracture that extends through the cryosphere into the briny aquifer. Brine will then fill this fracture to either the potentiometric surface or the level at which the diurnal and annual thermal wave drop the temperature below the eutectic temperature, which results in an ice dam. As northern spring approaches solar insolation/warming increases, eventually breaching the ice dam. The pent-up brine is released and the RSL flow downslope over the deeper ice-saturated regolith. Note that in the confined aquifer thesis, the fracture should be able to discharge at a faster rate initially in late winter as lateral recharge combined with no discharge would have allowed recovery of its potentiometric surface. The potentiometric surface falls back down to the surface of the source or spring (Fig. 13b) as brine is discharged throughout the season. This is consistent with the lengthening rate observations that show much large lengthening rates within the first 100 sols (Fig. 6).

A near-surface aquifer must be protected from evaporative loss (possibly by a low-permeability duricrust) or else recharged (Zent and Fanale, 1986). Hundreds of meters of ice-table recession is predicted for the low- and mid-latitudes (e.g., Squyres et al., 1992) and will be larger for the higher vapor pressure over water. The inference of buried ice beneath lobate debris aprons (Holt et al., 2008) indicates that mid-latitude ice can nonetheless be preserved (Parsons et al., 2011). Alternatively, hundreds of meters of water in the CAP region must be recharged by flow from the surrounding highlands during the Amazonian, with the net evaporative loss <1 m Global Equivalent Layer.

Briny aquifers are our preferred sources because they are both temperature-responsive (as observed RSL are) and able to annually provide a large volume of brine to the near-surface. As additional HiRISE-derived DTMs are generated for CAP RSL sites, the unconfined aquifer model can be tested by comparing the elevation of the RSL source regions to the elevation of the surrounding plains. We cannot determine if the aquifer under an RSL site is regional and linked to other RSL sites. However, one might expect that individual small heterogeneous aquifers would lose pressurization and drain more quickly than a regional aquifer. We assume that we are not witnessing a special time, and therefore suggest that the aquifer is regional and any steep-sided craters without RSL may not currently possess the proper plumbing (e.g., a permeable fracture that extends from the aquifer to the surface for the confined aquifer model). The extent of this regional aquifer may extend well beyond the CAP RSL sites, although it can only be constrained to below the sites of CAP RSL that lengthen, yielding a current aquifer area >190,000 km^2.

The depth and thickness of the aquifer is difficult to constrain given uncertainties in its initial and current salt content and type, heat flow, and subsurface thermal conductivity. There are four possible individual salts ($CaCl_2$, $Mg(ClO_3)_2$, $Mg(ClO_4)_2$, $Ca(ClO_4)_2$; Fig. 12b) that could be within the aquifer or more likely a mixture of these salts that have a eutectic temperature below the mean annual CAP temperature (220–225 K). Our proposed aquifer and RSL flow mechanisms require different freezing temperatures of 220–225 K and 238–252 K, respectively. We suggest that once the RSL begin to flow the loss of water to the atmosphere and/or the dissolving of remnant salt creates a super-eutectic concentration, which raises the freezing temperature of the RSL.

5.3. Comparison to other RSL regions

While CAP and SML RSL have some broad similarities, in detail they are very different. One would expect that the seasonality of CAP RSL would just be shifted by 180° in L_s, but it is not. The differences between these RSL geographic bands are primarily due to the significant change in distance between aphelion (1.666 AU at L_s 71°) and perihelion (1.381 AU at L_s 251°) of Mars' orbit. This causes northern summer surface temperatures to be colder (by ~25 K) than in the south. Therefore, we hypothesize that if the CAP RSL had the same source mechanism as the SML RSL, there would be no RSL in CAP. However, CAP RSL do exist because they are significantly more briny. For example, CAP and SML RSL begin to advance when observed afternoon surface temperatures are 240 ± 2 K and 296 ± 2 K (Stillman et al., 2014), respectively. Based on evaporite outcrops which are mostly found in the southern hemisphere (Osterloo et al., 2008, 2010) one would expect just the opposite. However, RSL are not surface flows, but instead flow in the very shallow subsurface. Furthermore, all four candidate salts for the briny aquifer hypothesis can deliquesce, and thus these salts could have percolated into the subsurface and been hidden from our spectral instruments. The considerable salt content of the CAP RSL also allows them to lengthen for a considerably longer period (369 ± 24 sols) than in the SML (~100 sols). Lastly, CAP RSL (4000 ± 200 m) are considerably lower in elevation than the SML RSL (3 ± 1000 m).

Stillman et al. (2014) found that SML RSL flow when afternoon temperature were >273 K and, based on water volumes, Grimm et al. (2014) suggested a freshwater aquifer source. However, subsurface temperatures would be below freezing with a highly insulating regolith. Fractures may control SML RSL discharge (Watkins et al., 2014) but freezing of fractures connecting to a freshwater aquifer is still problematic.

There is one SML RSL site that is anomalous (Hale Crater 35.7°S, 323.4°E, RSL elevations of about −1500 m) where this briny aquifer recharge mechanism might work. This site lengthens before and after the other typical SML RSL sites (starts and stops lengthening between L_s 148.5–193.5° and 329.7–341.9°, respectively; typical SML values are given in Table 1), has a mean annual temperature of ~215 K (Mellon et al., 2004), possesses two periods with differing lengthening rates (similar to the CAP RSL), and may have had shallow groundwater in the past (Andrews-Hanna and Lewis, 2011). Therefore, Hale Crater appears to behave more like a CAP RSL than an SML RSL.

The water budget estimate for CAP RSL of 1.5–5.6 m^3/m of headwall for a saturated flow depth of 2–6 cm is remarkably similar to the water budget estimate for SML RSL of 2–10 m^3/m for a saturated flow depth of 5 cm and 0.4–2 m^3/m for a saturated flow depth of 1.5 cm (Grimm et al., 2014). This SML estimate was hydraulically derived while our CAP approach is thermally derived. Furthermore, CAP RSL have a larger loss-to-storage ratio of 3.9 ± 2.1 and 6.1 ± 3.1 indicated for T_f = 238 and 252 K, respectively, than that of 1–3 for SML RSL (Grimm et al., 2014). CAP RSL have a larger loss-to-storage ratio because they reach equilibrium, while SML RSL flow has been interpreted as "slug" flow (Grimm et al., 2014) where the discharge rate is always greater than the sublimation and evaporation losses.

Comparisons of CAP RSL to the Valles Marineris (VM) and Equatorial Highlands RSL sites are premature. Valles Marineris contains the densest population of RSL (Fig. 1) and possesses the longest RSL on the planet. However, understanding VM RSL is complicated by the fact that their seasonality varies as a function of slope facing direction and dust events (McEwen et al., 2014a, 2014b) and lengthening occurs at the same time as fading (Stillman et al., 2015). Preliminary findings have estimated VM RSL water budgets to be significantly larger than SML or CAP RSL, briny, and likely recharged via a briny aquifer (Stillman et al., 2015), although the hydrogeology of such an aquifer remains challenging. The Equatorial Highlands now have three confirmed RSL sites, although little analysis has been conducted to date.

Lastly, we can offer no explanation as to why CAP RSL only form on southwest- and west-facing directions, while SML RSL are found on nearly all slope orientations (but favor north-, northwest-, and west-facing slopes; Stillman et al., 2014). CAP equatorial south-facing slopes should receive the most solar insolation, yet no RSL have been detected on these slopes. Furthermore, the south-facing slopes appear to be older with more craters on them and it is unclear if the RSL themselves are responsible for the removal of craters on their slopes or if other unknown mechanisms are responsible. Perhaps this older material is disrupting the RSL flow and/or recharge mechanism on south-facing slopes, at least during the current insolation conditions.

6. Conclusion

Our calculated CAP RSL water budget of 1.5–5.6 m^3/m of headwall suggests that water vapor transport cannot provide enough water to provide annual water or salt recharge. Therefore, we conclude that a briny aquifer is the only candidate mechanism that can provide ample annual brine recharge. We hypothesize that this aquifer was formed via subsurface flow from the surrounding highlands to the lowlands as part of a quasi-global system (Clifford and Parker, 2001; Andrews-Hanna and Lewis, 2011) that altered mineralogy at Meridiani Planum (e.g., Andrews-Hanna et al., 2010) and McLaughlin crater (Michalski et al., 2013). The aquifer could be a shallow unconfined aquifer or deeper confined aquifer. In either case the freezing temperature of the briny aquifer must be less than the mean annual surface temperature, allowing it be liquid at depth. During the coldest part of the year near-surface temperatures drop (L_s 224–337°), creating an ice dam. As temperatures warm, the ice dam is breached and brine discharges, forming the RSL. The RSL initially possess a high lengthening rate (>1.86 m/sol; Fig. 7a), possibly because of an initially high source discharge rate that later slows and/or evaporation and sublimation losses of the RSL are initially lower. Furthermore, the freezing temperature of the brine may be at its minimum value initially, as the salt concentration rises as the water fraction is increasingly lost. This suggests that the brine concentration within the RSL path is likely a super-eutectic concentration (Fig. 12). A super-eutectic concentration would then allow the brine to realize a temperature of precipitation of 238–252 K that is consistent with our 1D thermophysical modeling. As the RSL continue to flow, they are confined to the top 8 cm of the surface and melt and refreeze daily (Figs. 8–11). The RSL lengthening rate then decreases (∼0.25 m/sol; Fig. 7a) and around $L_s \sim 154°$ they likely reach an equilibrium where the evaporation and sublimation losses equal the discharge into the RSL. Around L_s 224° the ice dam at the source region reforms, discharge into the RSL stops, and as water sublimates away the albedo of the RSL fade. The salt within the RSL path must be removed so that it does not impede future flows.

We conclude that northern mid-latitude RSL only occur in CAP because this region is both low in elevation (but surrounded by higher elevations to the east, south, and west) and albedo, maximizing the probability of an aquifer-based, insolation-controlled discharge. Otherwise optimal sites with higher albedo and/or further to the north are devoid of RSL since they do not currently receive enough insolation to breach any subsurface ice dam. Although the anomalous SML RSL site at Hale Crater may be more similar to CAP RSL, in general CAP RSL are much different than SML RSL. CAP RSL start lengthening at considerably colder temperatures than SML RSL, indicating that CAP RSL are significantly more salty. Because CAP RSL can flow at such low temperatures they also flow for four times longer than SML RSL. Since CAP RSL flow for so long, their lengthening rate changes during the season, and eventually they reach an equilibrium phase where the amount of water being discharged equals the amount of water that is lost to evaporation and sublimation.

Overall, further HiRISE images that are closely spaced in time (∼15 sols) especially near the start and stop of lengthening can better constrain seasonal variations and possibly locate more CAP sites. Additionally, more complex subsurface models are needed to further model RSL, such as those that incorporate three-phase flow (including vadose zone effects that dominate the near-surface) and that can incorporate varying salt content as it changes throughout the season. However, in the end, a dedicated surface and/or orbital (Paige et al., 2012; McEwen et al., 2012) mission may be needed to fully understand these intriguing, globally-distributed features.

Acknowledgments

The work was performed under NASA Mars Data Analysis Grant NNH13ZDA001N. We would like to thank Chris Edwards and an anonymous reviewer for providing detailed and constructive reviews.

Appendix A. Supplementary material

Supplementary data associated with this article can be found, in the online version, at http://dx.doi.org/10.1016/j.icarus.2015.10.007.

References

Andrews-Hanna, J.C., Lewis, K.W., 2011. Early Mars hydrology: 2. Hydrological evolution in the Noachian and Hesperian epochs. J. Geophys. Res. 116, E02007.
Andrews-Hanna, J.C., Phillips, R.J., Zuber, M.T., 2007. Meridiani Planum and the global hydrology of Mars. Nature 446, 163–166. http://dx.doi.org/10.1038/nature05594.
Andrews-Hanna, J.C. et al., 2010. Early Mars hydrology: Meridiani playa deposits and the sedimentary record of Arabia Terra. J. Geophys. Res. 115, E06002. http://dx.doi.org/10.1029/2009JE003485.
Bryson, K.L. et al., 2008. Stability of ice on Mars and the water vapor diurnal cycle: Experimental study of the sublimation of ice through a fine-grained basaltic regolith. Icarus 196, 446–458.
Burt, D.M., Knauth, L.P., 2003. Electrically conducting, Ca-rich brines, rather than water, expected in the martian subsurface. J. Geophys. Res. 108. http://dx.doi.org/10.1029/2002JE001862.
Carr, M.H., 1979. Formation of martian flood features by release of water from confined aquifers. J. Geophys. Res. 84, 2995–3007.
Chevrier, V.F., Altheide, T.S., 2008. Low temperature aqueous ferric sulfate solutions on the surface of Mars. Geophys. Res. Lett. 35, L22101. http://dx.doi.org/10.1029/2008GL035489.
Chevrier, V.F., Rivera-Valentin, E.G., 2012. Formation of recurring slope lineae by liquid brines on present-day Mars. Geophys. Res. Lett. 39, L21202.
Chevrier, V.F. et al., 2009. Stability of perchlorate hydrates and their liquid solutions at the Phoenix landing site, Mars. Geophys. Res. Lett. 36, L10202.
Christensen, P.R., 1986. The spatial distribution of rocks on Mars. Icarus 68, 217–238.
Christensen, P.R. et al., 2001. Mars Global Surveyor Thermal Emission Spectrometer experiment: Investigation description and surface science results. J. Geophys. Res. 106, 23823–23872.
Christensen, P.R. et al., 2004. The Thermal Emission Imaging System (THEMIS) for the Mars 2001 Odyssey Mission. Space Sci. Rev. 110, 85–130.
Christensen, P.R. et al., 2009. JMARS – A Planetary GIS. <http://adsabs.harvard.edu/abs/2009AGUFMIN22A..06C>.
Clifford, S.M., Parker, T.J., 2001. The evolution of the martian hydrosphere: Implications for the fate of a primordial ocean and the current state of the northern plains. Icarus 154, 40–79.
Clifford, S.M. et al., 2010. Depth of the martian cryosphere: Revised estimates and implications for the existence and detection of subpermafrost groundwater. J. Geophys. Res. 115, E07001. http://dx.doi.org/10.1029/2009JE003462.
CRC Handbook of Chemistry and Physics, 2007–2008, 88th ed. CRC Press, Boca Raton, FL, pp. 8–52 to 8–77.
Davies, D.W., 1979. The relative humidity of Mars' atmosphere. J. Geophys. Res. 84 (B14), 8335–8340.
Dickson, J.L. et al., 2013. Don Juan, Pond Antarctica: Near-surface $CaCl_2$–brine feeding Earth's most saline lake and implications for Mars. Sci. Rep. 3, 1–7.
Farrell, W.M. et al., 2009. Is the martian water table hidden from radar view? Geophys. Res. Lett. 36, L15206. http://dx.doi.org/10.1029/2009GL038945.
Goldspiel, J.M., Squyres, S.W., 2011. Groundwater discharge and gully formation on martian slopes. Icarus 211, 238–258.
Gough, R.V. et al., 2011. Laboratory studies of perchlorate phase transitions: Support for metastable aqueous perchlorate solutions on Mars. Earth Planet. Sci. Lett. 312, 371–377.
Grimm, R.E., Painter, S.L., 2009. On the secular evolution of groundwater on Mars. Geophys. Res. Lett. 36, L24803. http://dx.doi.org/10.1029/2009GL041018.
Grimm, R.E. et al., 2014. Water budgets of martian recurring slope lineae. Icarus 233, 316–327.

Grotzinger, J.P. et al., 2005. Stratigraphy and sedimentology of a dry to wet eolian depositional system, Burns formation, Meridiani Planum, Mars. Earth Planet. Sci. Lett. 240, 11–72. http://dx.doi.org/10.1016/j.epsl.2005.09.039.

Haberle, R.M. et al., 2001. On the possibility of liquid water on present-day Mars. J. Geophys. Res. 106, 23317–23326.

Hanley, J. et al., 2012. Chlorate salts and solutions on Mars. Geophys. Res. Lett. 39, L08201.

Hashin, Z., Shtrikman, S., 1962. A variational approach to the theory of the effective magnetic permeability of multiphase materials. J. Appl. Phys. 33 (10), 3125–3131.

Hayne, P.O. et al., 2012. Carbon dioxide snow clouds on Mars: South polar winter observations by the Mars Climate Sounder. J. Geophys. Res. 117, E08014.

Hecht, M.H., 2002. Metastability of liquid water on Mars. Icarus 156, 373–386.

Holt, J.W. et al., 2008. Radar sounding evidence for buried glaciers in the southern mid-latitudes of Mars. Science 322, 1235–1238.

Ingersoll, A.P., 1970. Mars: Occurrence of liquid water. Science 168, 972–973.

Jaumann, R. et al., 2007. The High-Resolution Stereo Camera (HRSC) experiment on Mars Express: Instrument aspects and experiment conduct from interplanetary cruise through the nominal mission. Planet. Space Sci. 55, 928–952.

Kieffer, H.H., 2013. Thermal model for analysis of Mars infrared mapping. J. Geophys. Res.: Planets 118, 451–470.

Kirk, R.L. et al., 2008. Ultrahigh resolution topographic mapping of Mars with MRO HiRISE stereo images: Meter-scale slopes of candidate Phoenix landing sites. J. Geophys. Res. 113, E00A24. http://dx.doi.org/10.1029/2007JE003000.

Knauth, L.P., Burt, D.M., 2002. Eutectic brines on Mars: Origin and possible relation to young seepage features. Icarus 158, 267–271.

Kreslavsky, M., Head, J., 1999. Kilometer-scale slopes on Mars and their correlation with geologic units: Initial results from Mars Orbiter Laser Altimeter (MOLA) data. J. Geophys. Res. 104, 21911–21924.

Levy, J.S., 2012. Hydrological characteristics of recurrent slope lineae on Mars: Evidence for liquid flow through regolith and comparisons with Antarctic terrestrial analogs. Icarus 219, 1–4.

Levy, J.S. et al., 2010. Concentric crater fill in the northern mid-latitudes of Mars: Formation processes and relationships to similar landforms of glacial origin. Icarus 209, 390–404.

Marion, G.M., Catling, D.C., Kargel, J.S., 2003. Modeling aqueous ferrous iron chemistry at low temperatures with application to Mars. Geochim. Cosmochim. Ac. 67, 4251–4266.

Marion, G.M., Kargel, J.S., Catling, D.C., 2008. Modeling ferrous-ferric iron chemistry with application to martian surface geochemistry. Geochim. Cosmochim. Ac. 72, 242–266.

Martin-Torres, F.J. et al., 2015. Transient liquid water and water activity at Gale crater on Mars. Nat. Geosci. http://dx.doi.org/10.1038/NGEO2412.

Masse, M. et al., 2014. Spectroscopy and detectability of liquid brines on mars. Planet. Space Sci. 92, 136–149.

McCleese, D.J. et al., 2007. Mars Climate Sounder: An investigation of thermal and water vapor structure, dust and condensate distributions in the atmosphere, and energy balance of the polar regions. J. Geophys. Res. 112, E05S06. http://dx.doi.org/10.1029/2006JE002790.

McEwen, A.S. et al., 2007. Mars Reconnaissance Orbiter's High Resolution Imaging Science Experiment (HiRISE). J. Geophys. Res. 112, E05S02.

McEwen, A.S. et al., 2011. Seasonal flows on warm martian slopes. Science 333, 740–743.

McEwen, A.S. et al., 2012. Future orbital measurements needed to understand present-day liquid H_2O on the surface of Mars. In: Concepts and Approaches for Mars Exploration, June 12–14, Houston, TX, 2447.

McEwen, A.S. et al., 2014a. Recurring slope lineae in equatorial regions of Mars. Nat. Geosci. 7, 53–58.

McEwen, A.S. et al., 2014b. Active modern Mars: What is happening on the surface today? In: 8th International Conference on Mars, Pasadena, CA, July 14–18, 1147.

McEwen, A.S. et al., 2015. Recurring slope lineae on Mars: Atmospheric origin? In: European Planetary Science Conference, 10, 786.

Mellon, M.T., Phillips, R.J., 2001. Recent gullies on Mars and the source of liquid water. J. Geophys. Res. 106 (E10), 23165–23179.

Mellon, M.T. et al., 2004. The presence and stability of ground ice in the southern hemisphere of Mars. Icarus 169, 324–340.

Michaels, T.I., Rafkin, S.C.R., 2008. Meteorological predictions for candidate 2007 Phoenix Mars Lander sites using the Mars Regional Atmospheric Modeling System (MRAMS). J. Geophys. Res. 113, E00A07.

Michalski, J.R. et al., 2013. Groundwater activity on Mars and implications for a deep biosphere. Nature 6, 133–138.

Möhlmann, D.T.F., 2010. Temporary liquid water in upper snow/ice sub-surfaces on Mars? Icarus 207, 140–148.

Mustard, J.F., Cooper, C.D., Rifkin, M.K., 2001. Evidence for recent climate change on Mars from the identification of youthful near-surface ground ice. Nature 412, 411–414.

Newsom, H.E., Hagerty, J.J., Thorsos, I.E., 2001. Location and sampling of aqueous and hydrothermal deposits in martian impact craters. Astrobiology 1, 71–88.

Nuding et al., 2014. Deliquescence and efflorescence of calcium perchlorate: An investigation of stable aqueous solutions relevant to Mars. Icarus 243, 420–428.

Ojha, L. et al., 2014. HiRISE observations of recurring slope lineae (RSL) during southern summer on Mars. Icarus 231, 365–376.

Ojha, L. et al., 2015. Spectral evidence for hydrated salts in recurring slope lineae on Mars. Nat. Geosci. http://dx.doi.org/10.1038/ngeo2546.

Osterloo, M.M. et al., 2008. Chloride-bearing materials in the southern highlands of Mars. Science 319, 1651–1654.

Osterloo, M.M. et al., 2010. Geologic context of proposed chloride-bearing materials on Mars. J. Geophys. Res. 115, E10012.

Paige, D.A. et al., 2012. Orbiting observatory for studying hydrologically active regions on Mars. In: Concepts and Approaches for Mars Exploration, June 12–14, Houston, TX, 4235.

Parsons, R.A., Nimmo, F., Miyamoto, H., 2011. Constraints on martian lobate debris apron evolution and rheology from numerical modeling of ice flow. Icarus 214, 246–257.

Piqueux, S., Christensen, P.R., 2009. A model of thermal conductivity for planetary soils: 2. Theory for cemented soils. J. Geophys. Res. 114, E09006.

Piqueux, S. et al., 2015. Enumeration of Mars years and seasons since the beginning of telescopic exploration. Icarus 251, 332–338.

Pommerol, A. et al., 2013. Photometric properties of Mars soils analogs. J. Geophys. Res.: Planets 118, 2045–2072.

Prettyman, T.H. et al., 2004. Composition and structure of the martian surface at high southern latitudes from neutron spectroscopy. J. Geophys. Res. 109, E05001. http://dx.doi.org/10.1029/2003JE002139.

Rafkin, S.C.R., Haberle, R.M., Michaels, T.I., 2001. The Mars Regional Atmospheric Modeling System: Model description and selected simulations. Icarus 151, 228–256.

Rummel, J.D. et al., 2014. A new analysis of Mars "special regions": Findings of the second MEPAG Special Regions Science Analysis Group (SR-SAG2). Astrobiology 14, 887–968.

Schwenzer, S.P. et al., 2012. Puncturing Mars: How impact craters interact with the martian cryosphere. Earth Planet. Sci. Lett. 335–336, 9–17.

Sears, D.W.G., Chittenden, J.D., 2005. On laboratory simulation and the temperature dependence of the evaporation rate of brine on Mars. Geophys. Res. Lett. 32, L23203.

Smith, D.E. et al., 1999. The global topography of Mars and implications for surface evolution. Science 284, 1495–1503.

Squyres, S.W. et al., 1992. Ice in the martian regolith. In: Kieffer, H.H. et al. (Eds.), Mars. University of Arizona Press, Tucson, AZ, pp. 523–554.

Stillman, D.E., Grimm, R.E., 2011. Radar penetrates only the youngest geological units on Mars. J. Geophys. Res. 116, E03001. http://dx.doi.org/10.1029/2010JE003661.

Stillman, D.E., Olhoeft, G.R., 2008. Frequency and temperature dependence in electromagnetic properties of martian analog minerals. J. Geophys. Res. 113, E09005. http://dx.doi.org/10.1029/2007JE002977.

Stillman, D.E. et al., 2014. New observations of martian southern mid-latitude recurring slope lineae (RSL) imply formation by freshwater subsurface flows. Icarus 233, 328–341.

Stillman, D.E. et al., 2015. Seasonal water budget suggests that a Valles Marineris Recurring Slope Lineae (RSL) site must be recharged by an aquifer. Lunar Planet. Sci. 44, 2669.

Travis, B.J., Feldman, W.C., Maurice, S., 2013. A mechanism for bringing ice and brines to the near surface of Mars. J. Geophys. Res.: Planets 118, 877–890. http://dx.doi.org/10.1002/jgre.20074.

Wang, C., Manga, M., Hanna, J.C., 2006. Can freezing cause floods on Mars? Geophys. Res. Lett. 33, L20202. http://dx.doi.org/10.1029/2006GL027471.

Wang, A. et al., 2015. Formation of chloride hydrates via vapor–solid reaction at low-T – Implication for a H_2O-rich cryosphere in Mars subsurface and on other icy planetary bodies. Lunar Planet. Sci. 46, 2483.

Watkins et al., 2014. Structurally controlled subsurface fluid flow as a mechanism for the formation of recurring slope lineae. Lunar Planet. Sci. 45, 2911.

Zent, A.P., Fanale, F.P., 1986. Possible Mars brines: Equilibrium and kinetic considerations. J. Geophys. Res. 91 (B4), D439–D445.